Phase Diagram and Tie-Line Determination for the Ternary Mixture DOPC/eSM/Cholesterol

N. Bezlyepkina, R. S. Gracià, P. Shchelokovskyy, R. Lipowsky, and R. Dimova*
Max Planck Institute of Colloids and Interfaces, Potsdam, Germany

ABSTRACT We propose a novel, to our knowledge, method for the determination of tie lines in a phase diagram of ternary lipid mixtures. The method was applied to a system consisting of dioleoylphosphatidylcholine (DOPC), egg sphingomyelin (eSM), and cholesterol (Chol). The approach is based on electrofusion of single- or two-component homogeneous giant vesicles in the fluid phase and analyses of the domain areas of the fused vesicle. The electrofusion approach enables us to create three-component vesicles with precisely controlled composition, in contrast to conventional methods for giant vesicle formation. The tie lines determined in the two-liquid-phase coexistence region are found to be not parallel, suggesting that the dominant mechanism of lipid phase separation in this region changes with the membrane composition. We provide a phase diagram of the DOPC/eSM/Chol mixture and predict the location of the critical point. Finally, we evaluate the Gibbs free energy of transfer of individual lipid components from one phase to the other.

INTRODUCTION

In recent years, the prevailing view of cell membrane structure has gradually evolved from the fluid mosaic model proposed by Singer and Nicolson (1) to a heterogeneous membrane model that hypothesizes the existence of domains of lipids in the liquid-ordered (l_o) phase surrounded by lipids in the liquid-disordered (l_d) phase (2). The l_o domains (also called lipid rafts) are rich in cholesterol (Chol) and saturated lipids, and are thought to play an important role in regulation of cell processes (3,4).

To gain insight into the roles of individual membrane components, many groups have focused their efforts on establishing model membrane systems containing the lipid species of interest. Vesicles constitute a well-defined model system for studying basic biophysical properties and the behavior of more complex biological membranes. Giant unilamellar vesicles (GUVs) are a particularly practical biomimetic tool for displaying membrane behavior on the cell-size scale directly under the optical microscope (5,6).

In this work, we used GUVs composed of the three major lipid components of the outer leaflet of an animal cell plasma membrane: an unsaturated phospholipid represented by dioleoylphosphatidylcholine (DOPC), a saturated phospholipid represented by egg sphingomyelin (eSM), and Chol. The most obvious way to obtain multicomponent vesicles is to prepare them from lipid mixtures. However, with this method, the composition of the different vesicles in a batch can vary drastically depending on the individual vesicle history. For example, before observation, a phase-separated vesicle may have budded and the two daughter vesicles may have attained compositions that are different from the composition of the mother vesicle. Particularly strong deviations in the vesicle composition are observed for multicomponent lipid mixtures that are not fully miscible at the temperature of observation (7,8). To overcome this problem, we use an alternative means of arriving at a specific vesicle composition, i.e., we produce vesicles with domains via electrofusion of two vesicles made of two different fully miscible lipid mixtures, as proposed previously (9).

After electrofusion, the lipids in the newly created vesicle redistribute depending on the new membrane composition as described by the phase diagram. The latter specifies which phases are present as a function of composition, temperature, and pressure. Fig. 1 shows a tentative phase diagram for the ternary mixture of DOPC, SM, and Chol at room temperature as compiled from literature data (8,10–24) and our own measurements. The reported data were obtained from membranes containing different types of SM, such as eSM, brain SM, palmitoyl (16:0) SM, and stearoyl (18:0) SM; thus, compiling a phase diagram such as the one shown in Fig. 1 is not very accurate. However, the obtained phase boundaries (Fig. 1 *B*) can be used as a rough guide for the phase state of the membranes to be studied. The joint presentation of data for palmitoyl and eSM is partially justified by the well-defined chain-melting temperature of eSM, which is close to that of palmitoyl SM (25,26), and by the high content of palmitoyl chains in eSM. Data for stearoyl and brain SM were used to establish the phase boundaries in case data for eSM or palmitoyl SM were unavailable.

Submitted October 30, 2012, and accepted for publication February 19, 2013.

*Correspondence: Rumiana.Dimova@mpikg.mpg.de

R. S. Gracià's present address is Culgi B.V., Leiden, The Netherlands.

Editor: Paulo Almeida.

0006-3495/13/04/1456/9 $2.00

http://dx.doi.org/10.1016/j.bpj.2013.02.024

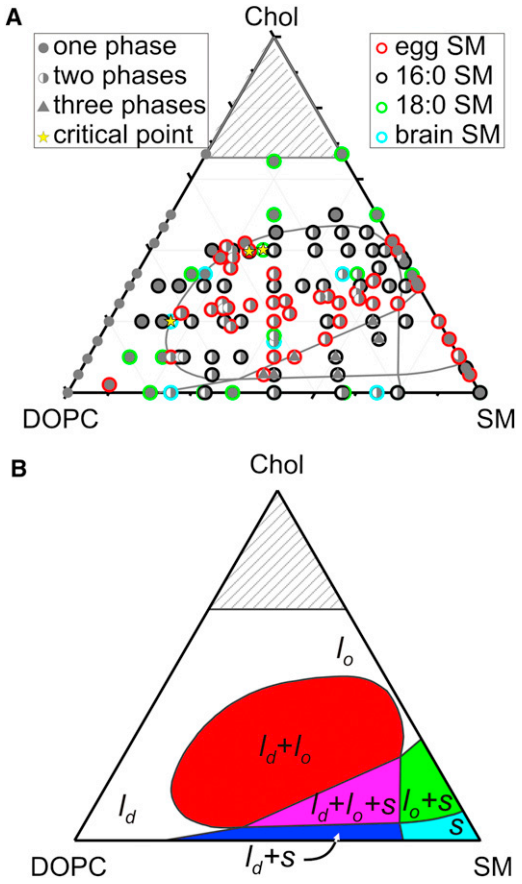

FIGURE 1 Phase diagram of the ternary mixture DOPC/SM/Chol at (23 ± 1)°C. (*A*) Data available in the literature (see text for references) and our own data were grouped according to the number of observed coexisting phases and SM type (see the two *insets*). Stars indicate reported critical points (see text for details). Tentative phase region boundaries deduced from the data are shown. A larger version of the graph is provided in the Supporting Material. (*B*) Rough estimate for the boundaries of one-, two-, and three-phase regions.

In Fig. 1 *A*, the data were grouped depending on the number of observed coexisting phases (one, two, or three) and on the SM type used (i.e., egg, brain, palmitoyl, or stearoyl SM). The stars indicate critical points reported in the literature (18,27,28). The solubility limit of Chol in phosphatidylcholine (PC) membranes was found to be 66–67 mol % (10). Above this concentration (*hatched region* in Fig. 1), Chol precipitates as monohydrate crystals and coexists with a lipid lamellar phase. At room temperature, eSM is in the gel or solid (s) phase, whereas DOPC is already in the fluid state at temperatures above −20°C. Below the solubility limit of Chol, mixtures of Chol and DOPC are fully miscible (14–16). At Chol fractions above ~30 mol %, the eSM/Chol membranes at room temperature are in the l_o state (29). At fractions between 8 mol % and 20–30 mol %, evidence for the coexistence of l_o/s in palmitoyl-SM/Chol membranes has been provided by differential scanning calorimetry (30,31) and fluorescence quenching studies (13). However, fluorescence microscopy observations of giant eSM/Chol vesicles demonstrated no phase coexistence region in this range (8), in similarity to results obtained with palmitoyl-SM/Chol mixtures (17). For the binary mixture eSM/Chol with a composition of 0/90/10 mol % (DOPC/eSM/Chol), giant vesicles appear to be in the solid phase (8). Note that further below, we will use the notation of DOPC/eSM/Chol in mol % for the membrane composition.

Knowing the boundaries of the regions in the phase diagram is not sufficient to characterize the composition of domains in a multicomponent vesicle. The domain composition is defined by the tie lines in the coexistence region. Locating the tie lines is challenging because the coexisting phases in the bilayer membrane cannot be physically isolated and then analyzed for chemical composition as is usually done, for example, with bulk solutions or alloys. So far, several methods have been applied to determine tie lines, including electron spin resonance spectroscopy (27,32,33), NMR spectroscopy (34–36), multiphoton fluorescence microscopy (37), fluorescence lifetime and anisotropy measurements (38), and low-angle x-ray scattering (39).

Here, we propose a new method for locating the tie lines in the liquid coexistence region of the phase diagram. It is based on microscopy quantification of the domain surface areas in giant vesicles produced by the fusion of two- or single-component vesicles. The method allows for direct observation of the membrane behavior under the microscope, and enables multiple tie lines to be located. In addition, one can evaluate the free energy of lipid transfer between the phases for each membrane component.

MATERIALS AND METHODS

Materials

The lipids used for vesicle preparation were 1,2-dioleoyl-*sn*-glycero-3-phosphocholine and eSM from Avanti Polar Lipids (Alabaster, AL), and Chol from Sigma (St. Louis, MO). All lipids were used without further purification, and stock solutions of lipids were stored in chloroform at –20°C until use.

The fluorescent probes 1,1′-dioctadecyl-3,3,3′,3′-tetramethylindocarbocyanine perchlorate ($DiIC_{18}$) and perylene were purchased from Molecular Probes (Leiden, The Netherlands) and Sigma-Aldrich (Steinheim, Germany), respectively. Dye stock solutions in chloroform were added to the lipid mixtures at concentrations of 0.1 mol % $DiIC_{18}$ or 0.4 mol % perylene. Perylene partitions preferentially in the l_o phase (11), whereas $DiIC_{18}$ favors the l_d phase (16).

Aqueous solutions of sucrose, glucose, sodium chloride (NaCl), and bovine serum albumin (BSA), all purchased from Sigma-Aldrich, were prepared with deionized water with a conductivity of 5.5 μS/m (Purelab Plus).

Vesicle preparation and observation

GUVs were prepared using the electroformation method described in Gracià et al. (40). In brief, a small volume (12–40 μl) of 4 mM lipid solution

in chloroform was spread on the surface of two preheated conductive glasses coated with indium tin oxide. The glasses were kept at 63–68°C in a vacuum drying oven (Heraeus Vacutherm VT 6025; Thermo Electron, Langenselbold, Germany) for at least 1 h to remove all traces of the organic solvent. The vesicles were grown at the same temperature to ensure that the lipids would be in the fluid phase and fully miscible. The two glasses were separated by a 2-mm-thick Teflon frame and assembled to form a chamber sealed with silicon grease. The chamber was filled with a sucrose solution (100 or 200 mOsm/kg). The solution osmolarities were measured with a cryoscopic osmometer (Osmomat 030; Gonotec, Germany). The conductive sides of the glasses were connected to an AC field function generator (Agilent 33220A; Agilent Technologies; Deutschland GmbH, Böblingen, Germany) and an alternating current of 1.1 V (peak-to-peak amplitude) at 10 Hz was applied for 1 h and then changed to 1.5 V at 5 Hz for another 2–5 h. In some cases, the frequency was changed to 1 Hz at the end to detach the vesicles from the glass.

For electrofusion experiments, the vesicle sucrose suspension was diluted with a mixture of 0.1 mM NaCl and glucose solution of slightly higher osmolarity than the osmolarity of the sucrose solution. This step slightly deflated the vesicles and created a sugar asymmetry between the interior and exterior of the vesicles. Due to the differences in density and refractive index between the sucrose and glucose solutions, the vesicles were stabilized by gravity at the bottom of the experimental chamber and had better contrast when observed with phase contrast microscopy.

Fluorescence microscopy snapshots were acquired with a confocal laser scanning microscope (Leica DM IRE2 or DMI 6000) using 20× Ph2 or 40× Ph2 objectives and laser excitation at 476 nm (argon laser) and at 561 nm (diode-pumped solid-state laser). Emission light was detected by a photomultiplier tube in spectral ranges of 480–533 nm (for perylene) and 564–654 nm (for $DiIC_{18}$). Electrofusion events were recorded nearly at the equatorial plane of the fusing vesicles as a time series, at approximately one image per 1.6 s (Leica DM IRE2) or one image per 0.14 s (Leica DMI 6000). For the domain formation and dynamics analysis, three-dimensional (3D) z-series of the vesicle with 0.33 μm increments were taken. To reduce possible artifacts that could arise from light-induced domain formation (41,42), illumination with low intensity was used and only a few 3D scans per vesicle were allowed. Under these conditions, no change in the size of the domains in equilibrated vesicles was observed. However, we cannot completely exclude possible effects associated with changes in the phase boundaries caused by the fluorescent dyes.

Micropipette aspiration

Micropipettes (inner diameter 5–30 μm) were prepared from glass capillaries (World Precision Instruments USA, Sarasota, FL) with the use of a micropipette puller (Sutter Instruments USA, Novato, CA) and their tips were shaped with a microforge (Narishige, Tokyo, Japan). Before use, each micropipette was coated with 1 mg/ml BSA solution to prevent vesicle adhesion to the glass. To apply suction pressure, the micropipettes were connected to water reservoirs mounted on two independent linear translational stages (M-531.DD; PI, Karlsruhe, Germany). Manipulation within the sample was achieved with the use of micromanipulators (MHW-103 and MLW-3; Narishige) secured to coarse manipulators (MMN-1; Narishige).

Vesicle electrofusion

For the electrofusion experiments, we used two vesicle populations: DOPC/Chol and eSM/Chol with a Chol concentration of 0–30 mol %. We mainly employed vesicles made of DOPC and Chol with compositions of 90/0/10 or 80/0/20 mol %, and vesicles made of eSM and Chol with a composition of 0/70/30 mol %. The DOPC/Chol membranes were stained with $DiIC_{18}$ (red false color in the confocal images), and the eSM/Chol membranes were labeled with perylene (green). We put ~50–100 μl of the DOPC/Chol and eSM/Chol vesicle suspensions into the observation chamber (see Fig. S2 of the Supporting Material) and diluted them ~10–20 times with glucose solution. The sample was left to equilibrate for 15–30 min. We then selected a pair of vesicles, one from each of the two populations, and applied an electric pulse to induce electrofusion after the vesicles had been brought together either by application of an alternating current or by means of micropipette aspiration. The field strength of the pulses was set to 110–300 V for 300 μs pulses or 200–300 V for 150 μs pulses. More details on the experimental procedure will be given elsewhere; a similar approach was already used for fusing two giant vesicles with the same membrane composition but different enclosed solutions to achieve nanoparticle synthesis in vesicles as closed containers (43). The electrofusion events were recorded by confocal microscopy.

The three-component vesicles thus obtained were observed after electrofusion, and 3D images of them were recorded. Two observation chambers were used. One was purchased from Eppendorf (Hamburg, Germany) and modified as described in the Supporting Material (see also Fig. S2, *A* and *B*). The other was made in house and used for electrofusion assisted with micropipettes (Fig. S2 *C*). The chambers were connected to a Multiporator (Eppendorf, Hamburg, Germany) that generated square-wave direct current (DC) pulses. The pulse strength and duration were set in the ranges of 5–300 V and 5–300 μs, respectively.

Image analysis

Leica Confocal Software, ImageJ, and in-house-written software were used for image analysis. The confocal series acquired after vesicle electrofusion were used to measure the surface areas of domains using an in-house-written plugin for ImageJ. An algorithm that is able to find the contour of the vesicle in the different slices using signal from both channels was developed (see Fig. 2 *A*). The shape of the vesicle was reconstructed from the contours from all slices, as shown in Fig. 2, *B* and *C*. Due to blur in images far from the equator, the upper part of the vesicle was fitted with a paraboloid; the lowest part was left flat because it corresponded to the coverslip. Occasionally, the original images were slightly skewed because of vesicle displacement in the chamber during recording of a 3D sections stack. The program corrected this by aligning the centers of the contours. Effects of possible aberrations were corrected as described in the Supporting Material.

The next step was to define the boundaries of the domains based on dye partitioning. Green color was assigned to the l_o phase labeled with perylene. Red color was assigned to the l_d phase labeled with $DiIC_{18}$. Perylene exhibited stronger photobleaching than $DiIC_{18}$. Because the green intensity was observed to decrease over the recording time, we used only the red channel to allocate the boundaries of the domains.

To determine the errors introduced by user handling during vesicle contour definition, two different investigators analyzed some of the images.

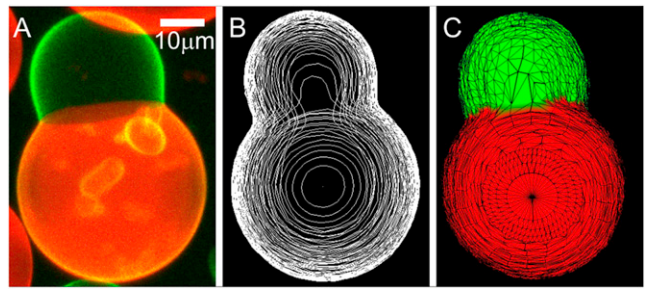

FIGURE 2 Reconstructing the 3D vesicle shape and domains from confocal images. (*A*) Maximum projection image of confocal 3D series (*top view*). The green color corresponds to the l_o phase and red indicates the l_d phase. (*B*) A set of contours from all slices. (*C*) A 3D model of the digitized vesicle surface.

Trends in domain surface fraction versus time were found to be independent of the investigator. The relative standard deviation (SD) of the domain area fractions was up to 2%. Error propagation calculations for the SD of the vesicle composition because of manual processing implied an estimate of maximum 2.0 mol % for each component.

The composition of the vesicle created by electrofusion was calculated from the measured domain areas (for details see the Supporting Material). Our estimates are based on the assumption that right after fusion, the compositions of the initial domains are still identical to the corresponding compositions of the two vesicles before fusion. We measure the initial area of these domains and, knowing the molecular surface area of each lipid in the different phases, calculate the respective number of molecules in the fused vesicle and consequently its composition. For the areas per lipid, we used available data interpolated to our conditions (51 $Å^2$ for SM (44), 27 $Å^2$ for Chol (44,45), and 70 or 66 $Å^2$ for DOPC in mixtures with 10 or 20 mol % of Chol (46,47), respectively). The composition error associated with the uncertainty in the values for the area per lipid was estimated to be maximum 0.6 mol % for an individual lipid (see Supporting Material for details).

Taking into account the errors from manual image processing and area per lipid uncertainty, the maximal SD in the vesicle composition was estimated to be 2.1 mol %.

RESULTS AND DISCUSSION

Compositional inhomogeneity of vesicles prepared from ternary lipid mixtures

The most commonly used method to obtain multicomponent vesicles is to prepare them directly from premixed lipid solutions. However, when prepared in this way, giant vesicles from the same batch can exhibit significant compositional differences, especially if their composition belongs to a region of phase coexistence (7,8,48,49). First, small compositional deviations between the vesicles could arise during the formation process (18). The growing vesicles are typically connected to the substrate via lipid tubes (43) with high membrane curvature, which may promote lipid sorting. Second, the membrane composition depends on the individual vesicle history, which is not known. Before a vesicle is observed under the microscope, budding of some part of the membrane might occur, which would change the overall composition of the vesicle. Generally, vesicles are formed at temperatures at which all components are fully miscible. Phase separation achieved by subsequent temperature quenching below the phase transition temperature of one of the components gives rise to a line tension of the domain boundary between the two phases, which can lead to budding (50). If the explored membrane composition is located close to the boundary of the region of coexisting phases, even small compositional deviations in the vesicle batch will affect the lipid miscibility. When observed by fluorescence microscopy, vesicles both with and without domains can be detected in the same batch (7) (see also Fig. 3 *A* and Fig. S3). For membrane compositions located deeper in the two-phase coexistence region, the deviations in the vesicle composition in a batch can be well demonstrated by the distribution of the area fraction of one of the domain types. If all vesicles had the same composition,

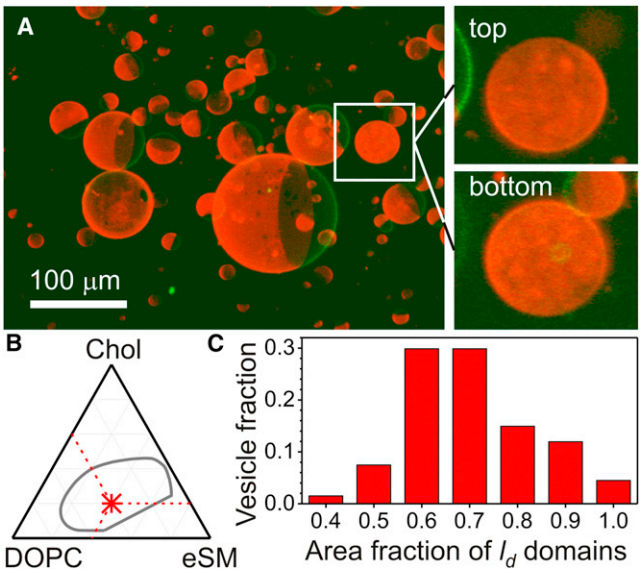

FIGURE 3 Compositional inhomogeneity of vesicles prepared from DOPC/eSM/Chol 40/40/20 observed at 23°C. (*A*) 3D projections reconstructed from confocal series. Vesicles with this composition exhibit phase separation, as observed for all vesicles on the image except for the framed one. This vesicle has no domains (see zoomed projections of the top and bottom vesicle hemispheres). (*B*) Membrane composition in the Gibbs triangle. The gray curve shows the boundary of the l_o-l_d coexistence region. (*C*) Distribution of the area fraction of red (l_d) domains over a population of ~70 vesicles from the same batch.

they should exhibit the same domain surface area fractions. However, the observed distribution of area fractions is often quite broad, as we show for vesicles made of DOPC/eSM/Chol 40/40/20. Inspection of Fig. 3 *C* shows that only 60% of the vesicles have nearly the same domain surface area ratio, i.e., nearly the same lipid composition. The obvious conclusion is that the composition of an observed vesicle made from the ternary lipid mixture can differ significantly from the composition of the starting lipid mixture used for the vesicle preparation.

Electrofusion of single- or two-component vesicles as a method to create three-component vesicles with well-defined compositions

To deal with the problem outlined in the previous section and to produce three-component vesicles with specific and precisely controlled composition, we established a new, to our knowledge, method as proposed earlier (9). Ideally, the scenario would be to fuse three single-component vesicles with certain areas. However, Chol by itself does not form a bilayer in an aqueous environment. Thus, we use a couple of vesicles, at least one of which contains Chol. The necessary condition to exclude deviations in the membrane composition during the formation of these vesicles is that the lipids in the starting mixtures are fully miscible at the working temperature (in this case, room

temperature). This approach lowers the complexity of the systems. Here, we used vesicles made of pure DOPC, DOPC/Chol (90/0/10 and 80/0/20), and eSM/Chol (0/80/20 and 0/70/30). The mixtures belong to regions in the phase diagram where no macroscopic phase separation is observed with fluorescence microscopy. Thus, by starting with single- or two-component homogeneous vesicles made of different lipids of known composition and forcing them to fuse with each other (e.g., via electrofusion), one can obtain three-component vesicles with precisely controlled composition. Of course, the size of the fusing vesicles affects the final vesicle composition.

The success of vesicle electrofusion depends on the membrane properties. It is generally assumed that fusion is initiated by localized membrane breakdown or electroporation (51). Therefore, to realize fusion, the vesicles have to porate at nearly the same parameters of the external field, i.e., they must have comparable values of the critical poration potential. The electroporation conditions for DOPC and SM membranes doped with Chol were found to be specific for the type of lipid and Chol content, as will be described elsewhere (see also Portet and Dimova (52)).

For successful electrofusion of two vesicles, the vesicles have to be correctly positioned, i.e., aligned in the field direction and in close contact at their poles facing the electrodes, because the probability of poration is highest at the poles. In the case of electrofusion of vesicles stabilized by gravity at the chamber bottom, it is only possible to fuse two vesicles of comparable size (within a difference of a few micrometers). We bring the vesicles together and align them by applying weak AC fields (an effect similar to that observed with cells that align in the field direction in pearl chains). An example of producing a two-domain vesicle by electrofusion is given in Fig. 4, *A–C*. Two single-phase vesicles are subjected to an electric pulse and fused. The resulting vesicle composition can be located precisely in the Gibbs triangle (Fig. 4 *D*).

When there are large differences in the sizes of the vesicles, or when two particular vesicles have been selected for fusion, the above protocol becomes ineffective. In this case, one can manipulate the vesicles, for example, by using micropipettes to bring them together and align them in the field direction. One can also apply this protocol to vesicles of arbitrary compositions by adjusting the membrane tension to match the vesicle poration thresholds. One example of electrofusion assisted by micropipettes is given in Fig. 4, *E–H*. In this example, the newly formed vesicle has a composition belonging to the single-phase (l_d) region in the phase diagram. The green domain quickly dissolves within ~5 min after fusion (see Fig. 4 *H*).

The examples given above demonstrate that by using the electrofusion method, one can create vesicles with compositions located anywhere in the phase diagram. This approach allows one to observe domain formation and dynamics, as well as to calculate the precise vesicle composition from the domain areas independently of the vesicle history.

Tie-line determination

As mentioned in the Introduction, several methods for tie-line determination have been previously reported. However, all of these methods have some shortcomings. Some of them involve the use of deuterated samples, which affects the hydrogen bonding in the system (53). Others are based on the use of bilayer stacks or multilamellar vesicles, and thus the bilayer hydration, interbilayer interactions, and/or interactions with the substrate can influence the results. Still others use small unilamellar vesicles, in which case membrane curvature might affect the thermodynamic behavior of the membranes. In addition, with nonimaging

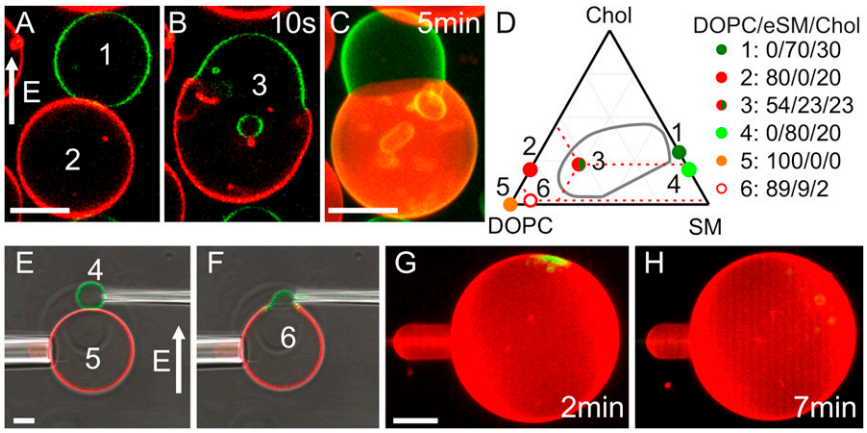

FIGURE 4 Electrofusion of single- or two-component vesicles provides a novel (to our knowledge) protocol to create three-component vesicles with precisely controlled composition. (*A–C*) Fusion of two freely suspended vesicles observed with confocal microscopy: cross sections (*A* and *B*) and a 3D projection (*C*). Vesicle 1 in panel *A* is composed of eSM/Chol (0/70/30). Vesicle 2 is made of DOPC/Chol (80/0/20). The two vesicles were subjected to an electric pulse (400 kV/m, 150 μs; arrow indicates the field direction) and fused to form vesicle 3 shown in *B* and *C*. The duration of time after application of the electric pulse is indicated in the upper-right corners. (*D*) Compositions of the vesicles in the images. The numbered compositions in the Gibbs triangle correspond to the numbered vesicles in *A*, *B*, *E*, and *F*. (*E–H*) Electrofusion of two vesicles brought into contact via micropipettes, as observed with an overlay of phase contrast images and confocal cross sections (*E* and *F*) or 3D projections (*G* and *H*). The initial vesicles differ significantly in size. Vesicle 4 is made of eSM/Chol (0/80/20) and has a radius of 17 μm. Vesicle 5 is composed of DOPC and has a radius of 52 μm. After application of an electric pulse (250 kV/m, 100 μs) the vesicles fuse to form vesicle 6, which is located in the single-phase region (*D*). The lipids mix quickly after the fusion, as shown in image *H*, which was taken 7 min after the pulse. All scale bars correspond to 20 μm.

methods, one cannot directly observe the sample to check that the vesicles have attained the same phase or exhibit similar area fractions for the different membrane domains. The only microscopy-based method that does not have these disadvantages is apparently so demanding that only a single tie line in the two-fluid-phase coexistence region can be located (37). Furthermore, the measurements are performed on giant vesicles prepared from ternary mixtures. As noted above, the composition of such vesicles is likely to vary over a wide range.

We propose a new, to our knowledge, method for tie-line determination in the l_o-l_d coexistence region of the phase diagram of ternary lipid mixtures. Three-component vesicles in this region were obtained via electrofusion of single- and/or two-component vesicles as explained above. Domain surface areas obtained from the 3D confocal scans recorded right after electrofusion were used to calculate the composition of the fused vesicle as described in "Image analysis" above and in the Supporting Material. The method for tie-line determination is based on quantifying the domain areas in the obtained three-component vesicle after equilibration. The mean equilibration time, beyond which the domain areas remain constant, was found to depend on the vesicle composition and was of the order of 30–120 min, being longer for vesicles with larger fraction of the l_o phase.

Briefly, the tie-line searching procedure involves the following steps: From the confocal image recorded right after fusion, we measure the domain surface areas and calculate the precise composition of the vesicle (see above). Then, we draw a hypothetical tie line through this composition point in the phase diagram. The intersection of this tie line with the phase boundary yields the hypothetical compositions of the two fluid phases. Taking the respective areas per molecule of the lipids in the phases, we calculate the hypothetical areas of the domains in the vesicle. If these areas correspond to the experimentally measured ones (taking into account the experimental accuracy), the hypothetical tie line can be considered a trial tie line (see the Supporting Material for a detailed protocol and a mathematical description of the searching procedure). In this way, several trial tie lines can be drawn through the composition point of the measured vesicle. The choice of valid tie lines can be then made under the conditions that 1), tie lines through different points do not cross each other inside the coexistence region; and 2), the boundary between the l_o-l_d two-phase and the s-l_o-l_d three-phase coexistence regions represents a tie line (called the end tie line).

Images of 13 fused vesicles exhibiting coexisting liquid phases were used to determine tie lines in the region of l_o-l_d coexistence. However, four out of 13 experimental points produced no valid trial tie lines. Thus, we questioned the reliability of the binodals for the l_o-l_d two-phase coexistence region as deduced from the literature data (see Fig. 1). The data in this region of the phase diagram were obtained predominantly from fluorescence microscopy experiments on giant vesicles. The uncertainty in the lipid composition of vesicles made from ternary lipid mixtures was estimated to be 2 mol % for each lipid species (18), suggesting similar uncertainty in the position of the coexistence curve in Fig. 1. Furthermore, most of the literature data are for 16:0 SM, whereas we used eSM. The vesicle preparation procedure could also affect the collected data (48).

To accommodate these uncertainties, we allowed for some adjustments of the binodals for the liquid-liquid coexistence region. By displacing the binodals in 0.5 mol % steps, we found that the first sets of valid trial tie lines for all 13 experimental points had a variation of 2 mol % from the binodal bounding the l_d region and 4.5 mol % from the one bounding the l_o region. Deviations >2 mol % from the l_d side were not considered, because this would leave some of the studied vesicle compositions outside the coexistence region. From the obtained nonintersecting trial tie lines, we selected a set that minimized the difference between the calculated and measured domain area fractions for the liquid-ordered or -disordered phases (see Fig. 5 and Supporting Material). We consider this set to be our best approximation of the tie-lines field. The exact coordinates of the tie lines determined in this way are given in Table S2.

Using the newly found tie-line end points, we revised the binodal facing the l_o-phase region as shown by the solid curve in Fig. 5. The shift of this binodal is understandable, considering that the majority of the experimental points used to define this binodal (as we initially did in Fig. 1)

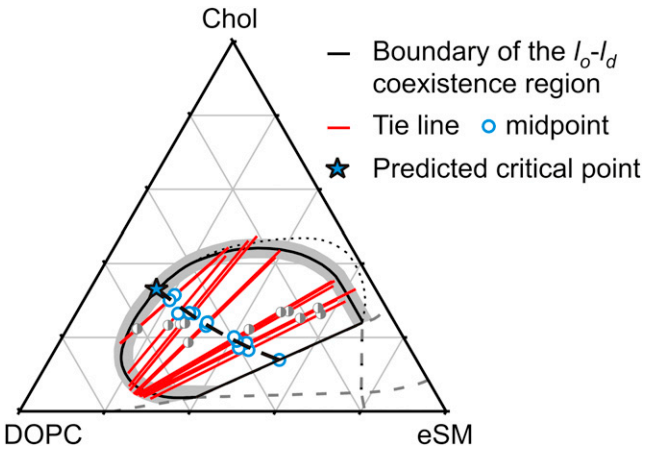

FIGURE 5 Phase diagram of the DOPC/eSM/Chol mixture at 23°C. Half-solid circles in gray indicate the compositions of the fused vesicles (see also Fig. S5 C) whose images were used to locate tie lines (*red*) within the l_o-l_d coexistence region. The latter region is indicated by the solid black curve shown with ±2 mol % deviation in gray (the *dotted black line* represents the initial binodal as defined in Fig. 1). The gray dashed lines show tentative boundaries for the rest of the phase coexistence regions. The blue open circles indicate the midpoints of the found tie lines, and the dashed black curve serves as a guide to the eye to connect them. It is extrapolated to the boundary of the l_o-l_d coexistence region to predict the location of the critical point as indicated by the star. At this critical point, the composition of the mixture is 52/15/33.

were obtained on 16:0 SM. Compared with 16:0 SM, eSM contains lipids with longer saturated chains that melt at higher temperature (the exact composition of eSM is 84% of 16:0 SM, 6% of 18:0 SM, 2% of 20:0 SM, 4% of 22:0 SM, and 4% of 24:0 SM eSM). Thus, it is to be expected that the presence of longer saturated chains will lead to an expansion of the l_o single-phase region at the expense of the l_o-l_d coexistence region. An analogous expansion can be observed when one compares the phase diagrams of DOPC/di16:0 PC/Chol (18) and DOPC/di18:0 PC/Chol (54).

From the binodals of the l_o-l_d coexistence region, and by applying the lever rule, we can also predict the approximate location of the critical point by extrapolating a curve passing through the midpoints of the found tie lines (see Fig. 5). The critical point deduced in this manner is located between those reported for the ternary mixtures with palmitoyl SM (18) and brain SM (27). It is closer to the former, which is to be expected given the compositional similarity of the lipids.

A compositional analysis of the l_o and l_d phases on the basis of our tie-line data (Table S2) reveals that in general, the l_o phase is mainly enriched in the saturated eSM and Chol, and the l_d phase is highly enriched in unsaturated DOPC (64–71 mol %) and further contains eSM and Chol but in much smaller amounts compared with the respective fractions in the l_o phase. The Chol content averages ~30–47 mol % in the l_o phase and 3–18 mol % in the l_d phase. On a qualitative level, our results agree well with published data suggesting that the l_o phase is strongly enriched in saturated lipids and moderately enriched in Chol, and the l_d phase is strongly enriched in unsaturated lipids (27,34,35).

Let us now consider the inclination of the tie lines as defined by their angle with respect to the compositional lines of constant Chol content. The end tie line toward the three-phase coexistence region has an angle of 24° (Table S2). The tie lines closest to the end tie line are approximately parallel to it. The angle of the subsequent tie lines increases up to 50° but then decreases to 41.5° for the two tie lines closest to the critical point. A similar nonmonotonous change in the inclination of the tie lines was previously reported for a DOPC/brain SM/Chol system (27). Such a behavior of the tie-line inclination does not seem to violate any thermodynamic rule for ternary mixtures, but it may also be related to the fact that many SM molecules with different chain composition are present in eSM and brain SM.

The inclinations of the tie lines are related to the difference in lipid mole fractions between each phase, which reflects the favorable or unfavorable interactions between the lipids. Relatively small tie-line inclinations imply a small difference in the Chol concentration and a large difference in the fractions of eSM and DOPC in the l_o and l_d phases. This might suggest that phase separation is driven by the interaction and alignment of eSM chains, leading to the exclusion of other lipids from the SM surroundings. Inclination angles close to 60° imply that the eSM concentration is similar in the two phases, whereas the mole fractions of DOPC and Chol differ significantly, which may indicate a steric incompatibility of DOPC and Chol. Our results suggest that the dominant mechanism of lipid phase separation in the coexisting l_o-l_d region depends on the particular membrane composition. When the DOPC amount averages half of the lipid content, the tie lines have a large inclination angle (up to 51°), implying that phase separation may be driven mainly by the steric incompatibility of DOPC and Chol. The decreasing slope of the tie lines closer to the end tie line at the three-phase coexistence region and those close to the critical point region suggests that in this case, phase separation may be driven mainly by the mutual attraction of eSM chains and the alignment of these chains.

Thermodynamics of lipid transfer

Our approach for creating multicomponent vesicles with known composition has a further advantage in that it enables us to characterize the thermodynamics of lipid mixing. After fusion, the vesicle composition is changed, followed by lipid redistribution via long-range diffusion. The driving force for this diffusion is the gradient in the chemical potentials of the lipids. At equilibrium, the chemical potential of each component has to be the same in every phase.

We refer to the initial domain that is enriched in DOPC immediately after fusion as the pre-l_d phase, and the domain that is initially enriched in eSM as the pre-l_o phase. From the initial domain compositions and the final equilibrated ones as specified by the tie lines, we conclude that DOPC diffuses from the pre-l_d domain to the pre-l_o domain, completing the formation of the l_o phase. eSM molecules diffuse in the opposite direction, contributing to the l_d phase formation. Quantitatively, the lipid transfer can be characterized in the following way. Based on the determined tie lines, we can evaluate the free energy of transfer between the phases for each lipid as (55,56):

$$\Delta G = -k_B T \ln K$$

Here, $k_B T$ is the thermal energy and K is the molar partition coefficient calculated as

$$K = \frac{\left([L]_{lo}/V^L_{lo}\right)}{\left([L]_{ld}/V^L_{ld}\right)}$$

where $[L]_{lo}$ and $[L]_{ld}$ are the mole fractions of lipid L in the l_o or l_d phases, respectively, and V^L_{lo} and V^L_{ld} are the volumes of the corresponding lipid phases. We define V^L_{lo} and V^L_{ld} as the sums of the products of the number of molecules and molecular volume of the corresponding lipid over all lipids located in the corresponding phase. The molecular volumes were taken as $V^{Chol}_{lo} \equiv V^{Chol}_{ld} = 630$ Å^3 for Chol, $V^{DOPC}_{lo} \equiv V^{DOPC}_{ld} = 1289$ Å^3 for DOPC, and $V^{eSM}_{lo} = 1165$ Å^3 and

$V_{ld}^{eSM} = 1176$ Å^3 for eSM depending on the Chol content (above or below 0.2 mol of Chol, respectively, corresponding to the l_o or l_d phase, respectively) (57). The values obtained for ΔG^{DOPC}, ΔG^{eSM}, and ΔG^{Chol} are of the order of 2 k_BT (see Table S2). The values of ΔG are negative for eSM and Chol but positive for DOPC. This means that partitioning from l_d into l_o is energetically favorable for eSM and Chol but energetically unfavorable for DOPC. The free energy of transfer ΔG is a measure of the relative affinity a particular lipid has to the l_o or l_d phase. The free-energy difference associated with thermodynamic fluctuations in an equilibrium system is typically of the order of the thermal energy, k_BT. The magnitudes of the free energies of transfer for DOPC and eSM are close to the magnitude of the thermal energy, suggesting that these molecules move between phases without a significant energy cost. On the other hand, the values of the free energy for Chol reveal a weak preference of Chol for the l_o phase. This implies that phase separation may have an impact on the sorting of Chol in cells.

CONCLUSIONS

We have shown that electrofusion of vesicles with different compositions provides a useful method for creating multicomponent vesicles with precisely controlled composition. The conventional method for vesicle electroformation produces vesicles with compositions that can vary over a wide range, as judged from the distribution in the area fraction of the domains. This variation is illustrated for vesicles made of DOPC/eSM/Chol 40/40/20 in Fig. 3. For this mixture, the average value and SD for the area fraction of red (l_d) domains is given by 0.71 ± 0.13. In contrast, the novel, to our knowledge, method developed here leads to an average value and SD for the area fraction of 0.62 ± 0.02 for the same ternary composition. Thus, the SD is reduced by more than a factor of 6. The remaining SD of ± 0.02 reflects the uncertainties in the estimates for the binodals and tie-line inclinations.

Using this electrofusion method, one can create vesicles with not only a precisely controlled composition but also a composition located anywhere in the phase diagram. Consecutive electrofusion events even allow one to create multidomain vesicles, as shown in Fig. S6.

By fusing two vesicles with different compositions and observing the lipid redistribution between the phases, we were able to establish a new (to our knowledge) method for tie-line determination. Our method is based on 1), knowing the precise composition of the vesicles before fusion; 2), measuring the surface areas of the different domains after fusion; and 3), matching tie lines and binodals by an iterative procedure. The approach is direct, facile, and not very experimentally demanding from an experimental viewpoint. It consists of quantifying the domain areas in vesicles recorded with confocal microscopy. We determined a set of tie lines in the l_o-l_d coexistence region of DOPC/eSM/Chol ternary membranes and predicted the tentative location for the critical point.

SUPPORTING MATERIAL

Supporting analysis, two tables, six figures, and references (58–60) are available at http://www.biophysj.org/biophysj/supplemental/S0006-3495(13)00241-5.

We thank C. Remde for help with confocal microscopy and image analysis.

REFERENCES

1. Singer, S. J., and G. L. Nicolson. 1972. The fluid mosaic model of the structure of cell membranes. *Science.* 175:720–731.
2. Simons, K., and E. Ikonen. 1997. Functional rafts in cell membranes. *Nature.* 387:569–572.
3. Edidin, M. 2003. The state of lipid rafts: from model membranes to cells. *Annu. Rev. Biophys. Biomol. Struct.* 32:257–283.
4. Simons, K., and W. L. C. Vaz. 2004. Model systems, lipid rafts, and cell membranes. *Annu. Rev. Biophys. Biomol. Struct.* 33:269–295.
5. Dimova, R., S. Aranda, …, R. Lipowsky. 2006. A practical guide to giant vesicles. Probing the membrane nanoregime via optical microscopy. *J. Phys. Condens. Matter.* 18:S1151–S1176.
6. Dimova, R. 2012. Giant vesicles: a biomimetic tool for membrane characterization. *In* Advances in Planar Lipid Bilayers and Liposomes. Academic Press, New York. 1–50.
7. Tian, A. W., B. R. Capraro, …, T. Baumgart. 2009. Bending stiffness depends on curvature of ternary lipid mixture tubular membranes. *Biophys. J.* 97:1636–1646.
8. Vequi-Suplicy, C. C., K. A. Riske, …, R. Dimova. 2010. Vesicles with charged domains. *Biochim. Biophys. Acta. Biomembranes.* 1798:1338–1347.
9. Lipowsky, R., and R. Dimova. 2003. Domains in membranes and vesicles. *J. Phys. Condens. Matter.* 15:S31–S45.
10. Huang, J. Y., and G. W. Feigenson. 1999. A microscopic interaction model of maximum solubility of cholesterol in lipid bilayers. *Biophys. J.* 76:2142–2157.
11. Baumgart, T., S. T. Hess, and W. W. Webb. 2003. Imaging coexisting fluid domains in biomembrane models coupling curvature and line tension. *Nature.* 425:821–824.
12. Baumgart, T., S. Das, …, J. T. Jenkins. 2005. Membrane elasticity in giant vesicles with fluid phase coexistence. *Biophys. J.* 89:1067–1080.
13. de Almeida, R. F. M., A. Fedorov, and M. Prieto. 2003. Sphingomyelin/phosphatidylcholine/cholesterol phase diagram: boundaries and composition of lipid rafts. *Biophys. J.* 85:2406–2416.
14. Filippov, A., G. Oradd, and G. Lindblom. 2003. Influence of cholesterol and water content on phospholipid lateral diffusion in bilayers. *Langmuir.* 19:6397–6400.
15. Filippov, A., G. Orädd, and G. Lindblom. 2003. The effect of cholesterol on the lateral diffusion of phospholipids in oriented bilayers. *Biophys. J.* 84:3079–3086.
16. Kahya, N., D. Scherfeld, …, P. Schwille. 2003. Probing lipid mobility of raft-exhibiting model membranes by fluorescence correlation spectroscopy. *J. Biol. Chem.* 278:28109–28115.
17. Veatch, S. L., and S. L. Keller. 2005. Miscibility phase diagrams of giant vesicles containing sphingomyelin. *Phys. Rev. Lett.* 94:148101.
18. Veatch, S. L., and S. L. Keller. 2005. Seeing spots: complex phase behavior in simple membranes. *Biochim. Biophys. Acta.* 1746:172–185.
19. Veatch, S. L., and S. L. Keller. 2003. Separation of liquid phases in giant vesicles of ternary mixtures of phospholipids and cholesterol. *Biophys. J.* 85:3074–3083.

20. Bacia, K., P. Schwille, and T. Kurzchalia. 2005. Sterol structure determines the separation of phases and the curvature of the liquid-ordered phase in model membranes. *Proc. Natl. Acad. Sci. USA.* 102:3272–3277.
21. Roux, A., D. Cuvelier, …, B. Goud. 2005. Role of curvature and phase transition in lipid sorting and fission of membrane tubules. *EMBO J.* 24:1537–1545.
22. Ayuyan, A. G., and F. S. Cohen. 2008. Raft composition at physiological temperature and pH in the absence of detergents. *Biophys. J.* 94:2654–2666.
23. Nyholm, T. K. M., D. Lindroos, …, J. P. Slotte. 2011. Construction of a DOPC/PSM/cholesterol phase diagram based on the fluorescence properties of trans-parinaric acid. *Langmuir.* 27:8339–8350.
24. Ionova, I. V., V. A. Livshits, and D. Marsh. 2012. Phase diagram of ternary cholesterol/palmitoylsphingomyelin/palmitoyloleoyl-phosphatidylcholine mixtures: spin-label EPR study of lipid-raft formation. *Biophys. J.* 102:1856–1865.
25. Mannock, D. A., T. J. McIntosh, …, R. N. McElhaney. 2003. Effects of natural and enantiomeric cholesterol on the thermotropic phase behavior and structure of egg sphingomyelin bilayer membranes. *Biophys. J.* 84:1038–1046.
26. Ramstedt, B., and J. P. Slotte. 1999. Comparison of the biophysical properties of racemic and d-erythro-N-acyl sphingomyelins. *Biophys. J.* 77:1498–1506.
27. Smith, A. K., and J. H. Freed. 2009. Determination of tie-line fields for coexisting lipid phases: an ESR study. *J. Phys. Chem. B.* 113:3957–3971.
28. Farkas, E. R., and W. W. Webb. 2010. Precise and millidegree stable temperature control for fluorescence imaging: application to phase transitions in lipid membranes. *Rev. Sci. Instrum.* 81:093704.
29. Wisniewska, A., and W. K. Subczynski. 2008. The liquid-ordered phase in sphingomyelincholesterol membranes as detected by the discrimination by oxygen transport (DOT) method. *Cell. Mol. Biol. Lett.* 13:430–451.
30. Estep, T. N., D. B. Mountcastle, …, T. E. Thompson. 1979. Thermal behavior of synthetic sphingomyelin-cholesterol dispersions. *Biochemistry.* 18:2112–2117.
31. Maulik, P. R., and G. G. Shipley. 1996. N-palmitoyl sphingomyelin bilayers: structure and interactions with cholesterol and dipalmitoylphosphatidylcholine. *Biochemistry.* 35:8025–8034.
32. Chiang, Y. W., J. Zhao, …, G. W. Feigenson. 2005. New method for determining tie-lines in coexisting membrane phases using spin-label ESR. *Biochim. Biophys. Acta.* 1668:99–105.
33. Swamy, M. J., L. Ciani, …, J. H. Freed. 2006. Coexisting domains in the plasma membranes of live cells characterized by spin-label ESR spectroscopy. *Biophys. J.* 90:4452–4465.
34. Veatch, S. L., I. V. Polozov, …, S. L. Keller. 2004. Liquid domains in vesicles investigated by NMR and fluorescence microscopy. *Biophys. J.* 86:2910–2922.
35. Veatch, S. L., K. Gawrisch, and S. L. Keller. 2006. Closed-loop miscibility gap and quantitative tie-lines in ternary membranes containing diphytanoyl PC. *Biophys. J.* 90:4428–4436.
36. Veatch, S. L., O. Soubias, …, K. Gawrisch. 2007. Critical fluctuations in domain-forming lipid mixtures. *Proc. Natl. Acad. Sci. USA.* 104:17650–17655.
37. Farkas, E. R., and W. W. Webb. 2010. Multiphoton polarization imaging of steady-state molecular order in ternary lipid vesicles for the purpose of lipid phase assignment. *J. Phys. Chem. B.* 114:15512–15522.
38. Castro, B. M., R. F. M. de Almeida, …, M. Prieto. 2007. Formation of ceramide/sphingomyelin gel domains in the presence of an unsaturated phospholipid: a quantitative multiprobe approach. *Biophys. J.* 93:1639–1650.
39. Uppamoochikkal, P., S. Tristram-Nagle, and J. F. Nagle. 2010. Orientation of tie-lines in the phase diagram of DOPC/DPPC/cholesterol model biomembranes. *Langmuir.* 26:17363–17368.
40. Gracià, R. S., N. Bezlyepkina, …, R. Dimova. 2010. Effect of cholesterol on the rigidity of saturated and unsaturated membranes: fluctuation and electrodeformation analysis of giant vesicles. *Soft Matter.* 6:1472–1482.
41. Ayuyan, A. G., and F. S. Cohen. 2006. Lipid peroxides promote large rafts: effects of excitation of probes in fluorescence microscopy and electrochemical reactions during vesicle formation. *Biophys. J.* 91:2172–2183.
42. Zhao, J., J. Wu, …, G. Feigenson. 2007. Phase studies of model biomembranes: macroscopic coexistence of L alpha plus L beta, with light-induced coexistence of L alpha plus Lo phases. *Biochim. Biophys. Acta.* 1768:2777–2786.
43. Yang, P., R. Lipowsky, and R. Dimova. 2009. Nanoparticle formation in giant vesicles: synthesis in biomimetic compartments. *Small.* 5:2033–2037.
44. Khelashvili, G. A., and H. L. Scott. 2004. Combined Monte Carlo and molecular dynamics simulation of hydrated 18:0 sphingomyelin-cholesterol lipid bilayers. *J. Chem. Phys.* 120:9841–9847.
45. Hofsäss, C., E. Lindahl, and O. Edholm. 2003. Molecular dynamics simulations of phospholipid bilayers with cholesterol. *Biophys. J.* 84:2192–2206.
46. Mathai, J. C., S. Tristram-Nagle, …, M. L. Zeidel. 2008. Structural determinants of water permeability through the lipid membrane. *J. Gen. Physiol.* 131:69–76.
47. Pan, J., S. Tristram-Nagle, …, J. F. Nagle. 2008. Temperature dependence of structure, bending rigidity, and bilayer interactions of dioleoylphosphatidylcholine bilayers. *Biophys. J.* 94:117–124.
48. Morales-Penningston, N. F., J. Wu, …, G. W. Feigenson. 2010. GUV preparation and imaging: minimizing artifacts. *Biochim. Biophys. Acta.* 1798:1324–1332.
49. Fidorra, M., A. Garcia, …, L. A. Bagatolli. 2009. Lipid domains in giant unilamellar vesicles and their correspondence with equilibrium thermodynamic phases: a quantitative fluorescence microscopy imaging approach. *Biochim. Biophys. Acta.* 1788:2142–2149.
50. Lipowsky, R. 1995. Bending of membranes by anchored polymers. *Europhys. Lett.* 30:197–202.
51. Neumann, E., A. E. Sowers, and C. Jordan. 1989. Electroporation and Electrofusion in Cell Biology. Plenum Press, New York.
52. Portet, T., and R. Dimova. 2010. A new method for measuring edge tensions and stability of lipid bilayers: effect of membrane composition. *Biophys. J.* 99:3264–3273.
53. Katsir, Y., Y. Shapira, …, E. Ben-Jacob. 2010. Entropic effects and slow kinetics revealed in titrations of D2O-H2O solutions with different D/H ratios. *J. Phys. Chem. B.* 114:5755–5763.
54. Zhao, J., J. Wu, …, G. W. Feigenson. 2007. Phase studies of model biomembranes: complex behavior of DSPC/DOPC/cholesterol. *Biochim. Biophys. Acta.* 1768:2764–2776.
55. Ben-Naim, A. 1978. Standard thermodynamics of transfer. Uses and misuses. *J. Phys. Chem.* 82:792–803.
56. Vitha, M. F., and P. W. Carr. 2000. The chemical meaning of the standard free energy of transfer: Use of van der Waals' equation of state to unravel the interplay between free volume, volume entropy, and the role of standard states. *J. Phys. Chem. B.* 104:5343–5349.
57. Greenwood, A. I., S. Tristram-Nagle, and J. F. Nagle. 2006. Partial molecular volumes of lipids and cholesterol. *Chem. Phys. Lipids.* 143:1–10.
58. Hell, S., and E. H. K. Stelzer. 1995. Lens aberrations in confocal fluorescence microscopy. *In* Handbook of Biological Confocal Microscopy. J. B. Pawley, editor.. Plenum Press, New York. 347–354.
59. Maulik, P. R., P. K. Sripada, and G. G. Shipley. 1991. Structure and thermotropic properties of hydrated N-stearoyl sphingomyelin bilayer membranes. *Biochim. Biophys. Acta.* 1062:211–219.
60. Smaby, J. M., M. M. Momsen, …, R. E. Brown. 1997. Phosphatidylcholine acyl unsaturation modulates the decrease in interfacial elasticity induced by cholesterol. *Biophys. J.* 73:1492–1505.

Phase diagram and tie-line determination for the ternary mixture DOPC/eggSM/Cholesterol

Supporting Material

N. Bezlyepkina, R. S. Gracià[†], P. Shchelokovskyy, R. Lipowsky and R. Dimova*

Max Planck Institute of Colloids and Interfaces, Science Park Golm, 14424 Potsdam, Germany

[†] Present address: Culgi B.V., P.O. Box 252, 2300 AG Leiden, The Netherlands
* Address correspondence to Rumiana.Dimova@mpikg.mpg.de

1. Phase diagram of the DOPC/SM/Chol mixture

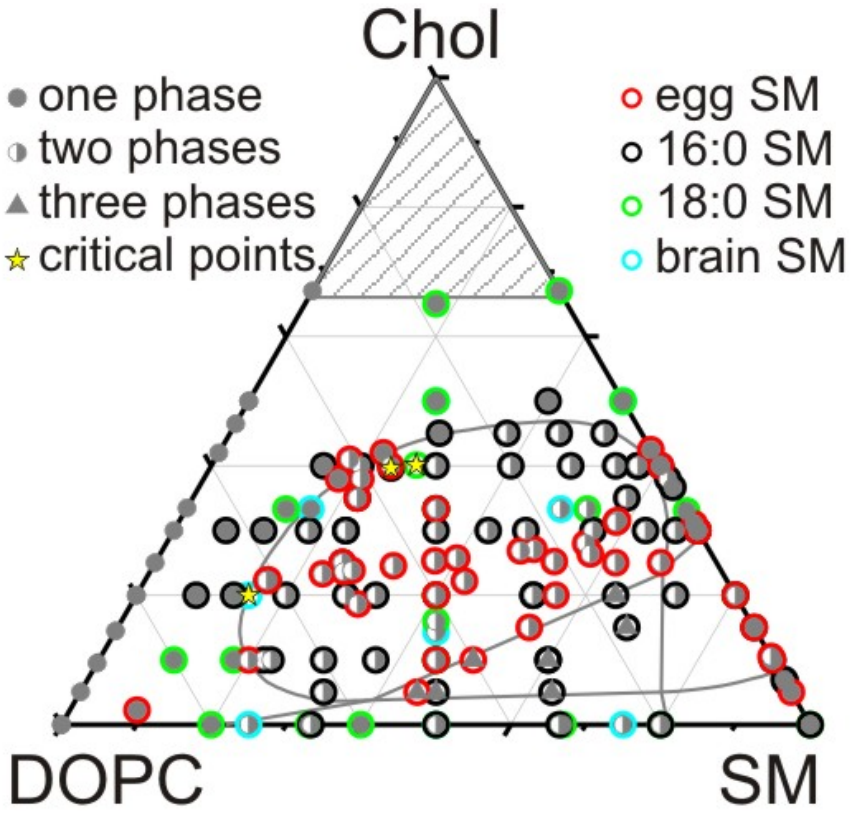

FIGURE S1 Phase diagram of the ternary mixture DOPC/SM/Chol at (23±1)°C. Data available in the literature (see main text for references) and our own data were grouped according to the number of observed coexisting phases (left legend) and SM type (right legend). Stars indicate reported critical points, see text for details. The figure represents a larger version of Fig. 1A in the main text.

2. Experimental chambers for vesicle electrofusion

Two observation chambers were used. One was purchased from Eppendorf (Hamburg, Germany) and modified as described below. The other was home-made and used for electrofusion assisted with micropipettes.

The original Eppendorf chamber consisted of a Teflon frame with a circular opening confined from below by a glass plate, see Fig. S2A. A pair of parallel platinum wires (92 μm in radius) with a gap distance of 500 μm was fixed to the glass. The thickness of the glass plate below the electrodes in the original chamber was lager then the working distance of the objectives used for recordings at the confocal microscope, which is why we removed the glass plate below the electrodes, see Fig. S2B. This has allowed the use of glass slides with the desired thickness. The vesicle solution was placed in the cavity of the observation chamber and closed with glass from above so that observation of the space between the electrodes was possible under the microscope in both fluorescence and transmission mode.

To create a suitable electrofusion chamber which allows for access of micropipettes, two Teflon frames of specially designed shape with fixed platinum electrode wires were used, see Fig. S2C. The platinum wires had a diameter of 0.2 mm or 0.5 mm. The Teflon frames were placed between two glass slides and fixed with silicon (CAF4, Rhone Poulenc, France). The space between the glass slides was about 5 mm. The chamber was open from two opposite sides to allow insertion of micropipettes.

The chamber was filled almost completely with glucose solution. The solutions of the different vesicle types were added afterwards from the different sides of the chamber. As such we had two vesicle reservoirs from which to select the vesicles with appropriate composition and size. The vesicles settled at the bottom of the observation chamber. A selected vesicle was weakly aspirated into a micropipette so that it was enough to hold and move it. Then, it was brought in close proximity to another aspirated vesicle in such a way that the axis connecting the centers of the external vesicle caps was perpendicular to the electrodes. Depending on the vesicle composition and size, the applied pressure could be varied to reach favorable electrofusion conditions.

The electrodes were connected by clips to the Multiporator to apply DC pulses. The distance between the electrodes was not constant for every chamber assembly since the electrodes were not parallel to each other but somewhat bent, see Fig. S2C, and this distance was adjusted by hand. To calculate the applied electric field, the distance between the electrodes was measured individually after each successful electrofusion event. When a given electric pulse has led to fusion, the pressure in one of the micropipettes was released so that the formed vesicle was held by one micropipette only.

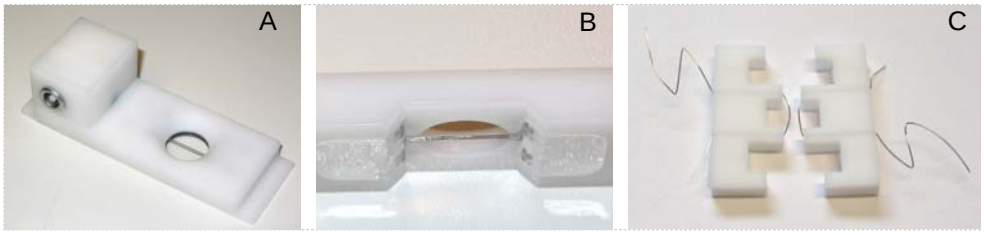

FIGURE S2 Electrofusion chambers. (A) Original Eppendorf chamber (top view); (B) Chamber modified for experiments at the confocal microscope (view from below); (C) The home-made chamber (without the covering glass slides) used for electrofusion with micropipette assistance.

3. Aberration corrections in the image analysis

By default, the home-made software for image analysis reconstructs the vesicle shape assuming the voxel to be cubic, i.e. taking the distance between the contours in the different slices to be the same as the pixel size, which is usually not true in confocal microscopy. In addition, spherical aberration may be introduced due to refractive index mismatch between the immersion medium and the specimen, deforming an image along the *z*-axis in three dimensional stack acquisitions. These aberrations can be corrected in the first approximation by simple rescaling of the *z*-axis in the data with the ratio of the refractive indices (1). To validate this approximation for our system Fluoresbrite YG 20.0 micron microspheres (Polysciences Inc., excitation 441 nm, emission 486 nm, d = 18.6±2.53 μm) were used to measure the particle size distortion along the *z*-axis in different media and with different objectives. The image of a particle in the *xz* plane (vertical cross section) was recorded with the confocal microscope. The particle diameters d_x and d_z as measured along the *x*- and the *z*-axis were found. Their ratio, d_x/d_z, was compared with the ratio of the refractive indices of the sample medium, n_s, and of the immersion medium, n_{imm}. Results of these measurements confirmed that those ratios are in close agreement, within a relative error of 8%. Thus, the correction factor Z_{corr} used for the *z*-axis rescaling of the vesicle images in the home-made software was calculated as the product of the ratio a_z/a_x between the axial and the lateral voxel sizes, a_z and a_x, respectively, (these were taken from the Leica microscope control software) and of ratio of the sample and immersion media refractive indices, $Z_{corr} = (a_z/a_x) \times (n_s/n_{imm})$.

4. Calculating the precise composition of a vesicle obtained by electrofusion

To determine the vesicle composition from the domain areas, we used the following procedure. From the first confocal series recorded right after the electrofusion event, we measured the surface areas of the green (l_o phase) and the red (l_d phase) domains, S_{green} and S_{red}, respectively. Since lipid redistribution usually takes longer than tens of minutes, we assumed that the composition of each domain in this first confocal series is identical to the corresponding compositions of the initial vesicles before fusion. For the green domain, we denote the mole fractions of SM and Chol with $f_{SM,\,initial}$ and $f^{lo}_{Ch,\,initial}$ respectively. For the red domain, we denote the mole fractions of DOPC and Chol with $f_{DOPC,\,initial}$ and $f^{ld}_{Ch,\,initial}$, respectively. From literature data on the areas per molecule for SM, Chol and DOPC, the area of the domains and their initial composition, we can calculate the exact composition of the fused vesicle as explained further below.

We denote the molecular surface area of each lipid in the different phases as A^{lo}_{SM} for eSM in the l_o phase, A^{ld}_{DOPC} for DOPC in the l_d phase, and A^{lo}_{Ch} and A^{ld}_{Ch} for Chol in the l_o and the l_d phase, respectively. We calculate the respective number of molecules, N_{SM}, N_{DOPC}, and N_{Ch}, in the vesicle produced by electrofusion as follows:

$$N_{SM} = \frac{S_{green}}{A_{SM}^{lo} + \frac{f_{Ch,initial}^{lo}}{f_{SM,initial}} A_{Ch}^{lo}}, \quad N_{DOPC} = \frac{S_{red}}{A_{DOPC}^{ld} + \frac{f_{Ch,initial}^{ld}}{f_{DOPC,initial}} A_{Ch}^{ld}},$$

$$N_{Ch} = \frac{S_{green}}{A_{Ch}^{lo} + \frac{f_{SM,initial}}{f_{Ch,initial}^{lo}} A_{SM}^{lo}} + \frac{S_{red}}{A_{Ch}^{ld} + \frac{f_{DOPC,initial}}{f_{Ch,initial}^{ld}} A_{DOPC}^{ld}}. \quad (1)$$

The total number of molecules is:

$$N = N_{SM} + N_{Ch} + N_{DOPC}. \quad (2)$$

Finally, the lipid mole fractions in the final vesicle, f_{SM}, f_{DOPC}, and f_{Ch}, i.e., the vesicle composition, will be:

$$f_{SM} = \frac{N_{SM}}{N} \times 100\%, \; f_{DOPC} = \frac{N_{DOPC}}{N} \times 100\% \text{ and } f_{Ch} = \frac{N_{Ch}}{N} \times 100\%. \quad (3)$$

There are three possible sources of errors in the calculation of the vesicle composition: error in measuring the surface areas of the domains in the fused vesicle (S_{green} and S_{red}), uncertainty of the area per molecule of the different lipids in the initial vesicles (A_{SM}^{lo}, A_{DOPC}^{ld}, A_{Ch}^{lo} and A_{Ch}^{ld}) and error due to imperfect compositions of these vesicles (i.e., error in $f_{SM,initial}$, $f_{Ch,initial}^{lo}$, $f_{DOPC,initial}$ and $f_{Ch,initial}^{ld}$). We neglect the latter error source, since the vesicles were prepared and stored at temperature at which the lipid components where fully miscible. We are then left with two error sources that we consider to be independent: the error stemming from the image processing procedure to extract the domain areas and the uncertainty of areas per lipid molecule.

Image processing: The vesicles are digitized by manual processing of confocal stacks. Thus, the main source of error comes from manually assigning contours to vesicle slices, since the software gives only approximate guides to help the human processing. In order to estimate the associated error, two authors of this study independently digitized 9 vesicles to measure domain areas and these sets of values were used to calculate the lipid composition (for fixed areas per lipid molecules). The maximal standard deviation was then calculated to be 2% of the mean for the domain area fractions and for the lipid composition 2.0 mol% for DOPC, 1.8 mol% for SM and 0.3 mol% for Chol as obtained from analytical estimates for error propagation. We take the largest of these three (2.0 mol% for DOPC) as the estimate of the error due to manual image processing and vesicle digitalization.

Areas per lipid molecule: There are no systematic data about how the areas per lipid change with membrane composition. Thus, we used values interpolated to our conditions from the data available in the literature (2-7): 51 Å^2 for SM (3), 27 Å^2 for cholesterol (3, 4), 70 or 66 Å^2 for DOPC with 10 or 20 mol% of Chol (5, 6), respectively. We varied the area per molecule in the ranges 46 – 53 Å^2 for SM, 25 – 31 Å^2 for Chol, 70 – 72 Å^2 for DOPC when mixed with 10 mol % Chol, and 66 – 68 Å^2 for DOPC when mixed with 20 mol % of Chol. To evaluate the error in the vesicle composition associated with the uncertainty in the areas per lipid, we performed Monte-Carlo simulation of the error propagation. From each of the above-indicated ranges for the lipid area per molecule, we drew 1 million samples assuming uniform distribution and calculated the corresponding vesicle composition and the standard deviation for all 13 vesicles analyzed. The standard deviation of the vesicle composition associated with the uncertainty in the lipid area per molecule was found to be 0.6 mol% for DOPC, 0.5 mol% for SM and 0.1 mol% for Chol as averaged between the vesicles. We also tested other ranges for the areas per lipid. If we take the values of the area per lipid as indicated in the main

text (see also Table S1), and allow a deviation of ±1 Å^2 for all three lipids, by the procedure above we get 0.2 mol% average standard deviation, ±2 Å^2 deviation produces 0.4 mol% average standard deviation and ±3 Å^2 deviation results in 0.6 mol% average standard deviation.

Total error: We consider the two error contributions described above to be statistically independent. Then, the total standard deviation of the lipid composition can be estimated by taking the square root of the sum of the squared standard deviations of the contributing errors. Combining data from Monte-Carlo simulations of the error propagation for the area per lipid and analytical results for the error propagation for the image processing we estimate the standard deviations in the composition to be 2.1 mol% for DOPC, 1.9 mol% for SM and 0.3 mol% for Chol. We have also performed the Monte-Carlo simulation with all parameters randomized – with the lipid areas uniformly distributed, as described above, and with the domain areas normally distributed with mean value and standard deviation as estimated by our two-user analysis. This approach produced estimation of the total standard deviation of the composition to be 2.1 mol% for DOPC, 1.7 mol% for SM and 0.3 mol% for Chol. As these two ways of the error estimate produce similar results, we use the largest of these values (2.1 mol% for DOPC) as a general estimation of the accuracy of our method with respect to the lipid composition of the final vesicle.

5. Compositional inhomogeneity of vesicles prepared from ternary lipid mixtures

Figure S3 illustrates the compositional inhomogeneity of vesicles prepared from a ternary lipid mixture located close to the boundary of the l_o-l_d coexistence region.

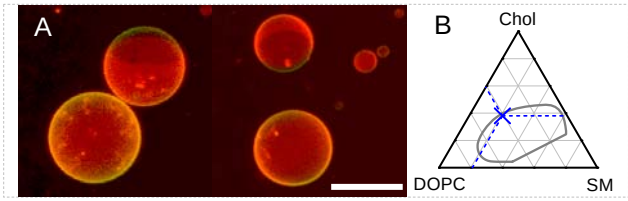

FIGURE S3 Compositional inhomogeneity of vesicles prepared from DOPC/eSM/Chol (41/21/38) mixture. (A) Two snapshots of 3D projections made from confocal series. Vesicles with domains (upper parts of the images) and vesicles without domains (lower parts of the images) coexist in the same sample. The scale bar is 50 μm. (B) Lipid composition (blue cross) in the Gibbs triangle. The grey curve shows the boundary of the l_o-l_d coexistence region.

6. Tie-line search procedure

The boundary of the region of l_o-l_d coexistence was represented as a polygon of 70 connected points. The proposed tie-line determination method consists of the following steps.

Step 1: Draw a line through the point corresponding to the vesicle composition on the phase diagram – we term this tie line "a hypothetical tie line" (Fig. S4). Read the coordinates at the intersections of the hypothetical tie line with the l_o-l_d region boundary. These coordinates yield the

compositions of the liquid ordered $\left\{ f_{DOPC}^{l_o}, f_{SM}^{l_o}, f_{Ch}^{l_o} \right\}$ and the liquid disordered $\left\{ f_{DOPC}^{l_d}, f_{SM}^{l_d}, f_{Ch}^{l_d} \right\}$ phases, where $f_{DOPC}^{l_i}, f_{SM}^{l_i}$ and $f_{Ch}^{l_i}$ are the mole fractions of the respective molecules in the corresponding phase (here l_i indicates either the l_o or the l_d phase).

Step 2: Calculate the surface areas of the phases according to the hypothetical tie line, $S_{tie\,line}^{lo}$ and $S_{tie\,line}^{ld}$, as sums of the surface areas occupied by all molecules in the corresponding phase:

$$S_{tie\,line}^{lo} = N_{SM}^{lo} A_{SM}^{lo} + N_{Ch}^{lo} A_{Ch}^{lo} + N_{DOPC}^{lo} A_{DOPC}^{lo} \tag{4a}$$

$$S_{tie\,line}^{ld} = N_{SM}^{ld} A_{SM}^{ld} + N_{Ch}^{ld} A_{Ch}^{ld} + N_{DOPC}^{ld} A_{DOPC}^{ld} \tag{4b}$$

where $A_{SM}^{lo}, A_{Ch}^{lo}, A_{DOPC}^{lo}$ and $A_{SM}^{ld}, A_{Ch}^{ld}, A_{DOPC}^{ld}$ are the corresponding molecular surface areas of the lipids in the l_o or l_d phase; $N_{SM}^{lo}, N_{Ch}^{lo}, N_{DOPC}^{lo}$ and $N_{SM}^{ld}, N_{Ch}^{ld}, N_{DOPC}^{ld}$ are the numbers of molecules in the l_o or l_d phase that can be calculated as follows.

The areas per molecule for the lipids in the different phases are given in Table S1. For the molecular area of DOPC in Eq. (4a-b), we have assumed a linear dependence on the cholesterol content and have taken interpolated values from data in the literature.

Table S1 Molecular surface areas of the different lipids used for the calculations of surface areas of the phases according to the hypothetical tie lines. The values correspond to room temperature.

Lipid	Area, Å^2	References
DOPC	71	(5-7)
+ 10 mol% Chol	70	
+ 20 mol% Chol	66	
+ 30 mol% Chol	66	
+ 40 mol% Chol	63	
SM	45	(2, 3)
+ 30 mol% Chol	51	
Chol	27	(3, 4)

The fraction of SM molecules in the l_o or l_d phases is defined as the ratio of the SM molecules number to the number of all molecules, N^{lo} or N^{ld}, in the corresponding phase:

$$f_{SM}^{lo} = \frac{N_{SM}^{lo}}{N^{lo}} \tag{5a}$$

$$f_{SM}^{ld} = \frac{N_{SM}^{ld}}{N^{ld}} \tag{5b}$$

The total number of SM molecules in the vesicle is a sum of the number of SM molecules in the l_o and l_d phases or is a product of the total number of lipids and the fraction of SM molecules in the vesicle:

$$N_{SM} = N_{SM}^{lo} + N_{SM}^{ld} \equiv N f_{SM} \tag{6}$$

From Eqs. (5 – 6) the number of SM molecules in the l_o phase is:

$$N_{SM}^{lo} = f_{SM}^{lo} N^{lo} \equiv N_{SM} - N_{SM}^{ld} \tag{7a}$$

$$N_{SM} - N_{SM}^{ld} = N_{SM} - f_{SM}^{ld} \left(N - N^{lo} \right) \tag{7b}$$

$$N^{lo} = \frac{N_{SM} - f_{SM}^{ld} N}{f_{SM}^{lo} - f_{SM}^{ld}} = N \frac{f_{SM} - f_{SM}^{ld}}{f_{SM}^{lo} - f_{SM}^{ld}} \tag{7c}$$

$$N_{SM}^{lo} = f_{SM}^{lo} N^{lo} = f_{SM}^{lo} N \frac{f_{SM} - f_{SM}^{ld}}{f_{SM}^{lo} - f_{SM}^{ld}} \tag{7d}$$

Then, the number of SM molecules in the l_d phase is

$$N_{SM}^{ld} = N_{SM} - N_{SM}^{lo} = N_{SM} - f_{SM}^{lo} N \frac{f_{SM} - f_{SM}^{ld}}{f_{SM}^{lo} - f_{SM}^{ld}} \tag{8}$$

The total number of molecules $\{N_{SM}, N_{Ch}, N_{DOPC}\}$ and the composition of the vesicle $\{f_{SM}, f_{Ch}, f_{DOPC}\}$ was calculated from the confocal images recorded right after the vesicle electrofusion as described in Section 4 of the Supporting Material.

The numbers of cholesterol and DOPC molecules in the corresponding phases are calculated in a similar fashion yielding:

$$N_{Ch}^{lo} = f_{Ch}^{lo} N \frac{f_{Ch} - f_{Ch}^{ld}}{f_{Ch}^{lo} - f_{Ch}^{ld}} \tag{9a}$$

$$N_{Ch}^{ld} = N_{Ch} - f_{Ch}^{lo} N \frac{f_{Ch} - f_{Ch}^{ld}}{f_{Ch}^{lo} - f_{Ch}^{ld}} \tag{9b}$$

$$N_{DOPC}^{lo} = f_{DOPC}^{lo} N \frac{f_{DOPC} - f_{DOPC}^{ld}}{f_{DOPC}^{lo} - f_{DOPC}^{ld}} \tag{10a}$$

$$N_{DOPC}^{ld} = N_{DOPC} - f_{DOPC}^{lo} N \frac{f_{DOPC} - f_{DOPC}^{ld}}{f_{DOPC}^{lo} - f_{DOPC}^{ld}} \tag{10b}$$

Step 3: From the areas of the phases estimated from the hypothetical tie line, $S_{tie\,line}^{lo}$ and $S_{tie\,line}^{ld}$, and those measured from the confocal image of the vesicle after equilibration, S_{eq}^{lo} and S_{eq}^{ld}, calculate the differences $\Delta\overline{s}$ between the hypothetical and measured domain area fractions for the liquid ordered or disordered phases:

$$\Delta\overline{s} = \left| \frac{S_{tie\,line}^{ld}}{S_{tie\,line}^{ld} + S_{tie\,line}^{lo}} - \frac{S_{eq}^{ld}}{S_{eq}^{ld} + S_{eq}^{lo}} \right| \equiv \left| \frac{S_{tie\,line}^{lo}}{S_{tie\,line}^{ld} + S_{tie\,line}^{lo}} - \frac{S_{eq}^{lo}}{S_{eq}^{ld} + S_{eq}^{lo}} \right|.$$

Step 4: Apply the selection criterion $\Delta\overline{s} < 2\%$, as set by the uncertainty in surface area measurements resulting from manual processing. If this selection criterion is fulfilled, i.e., the hypothetical tie line becomes a trial tie line, proceed to the following step. If not, draw another hypothetical tie line and repeat the procedure from Step 1.

Step 5: From all trial tie lines found for each measured vesicle composition, make a choice in such a way that:

i) The boundary between the region of l_o-l_d coexisting phases and the region of s-l_o-l_d coexisting phases represents a tie line (called the end tie line).

ii) Tie lines do not cross each other inside the l_o-l_d coexistence region.

The search procedure is illustrated in Fig. S4. The procedure was automated with the help of home-written software.

To draw the hypothetical tie lines in the l_o-l_d region of the phase diagram, a series of lines with 1 degree of arc increment in slope angle was plotted through the selected composition point. The corresponding hypothetical domain surface areas were calculated for each line. After applying the selection criteria in Step 4 and the rules in Step 5 in the search procedure, we obtain the coordinates of the trial tie lines. Examining all composition points of the equilibrated fused vesicles, no trial tie lines for 4 out of the 13 composition points were found for the defined coexistence curve.

We then allowed for some deviation from the defined coexisting curve and the procedure was repeated. Deviation from the coexistence curve was done with a step of 0.5 mol% both inward and outward along the trial direction. All possible combinations of inward and outward deviations for both hypothetical tie-line ends were tested for acceptance. Thus, several line segments on each line plotted through the composition point were taken to calculate the fraction surface areas. The number of line segments and their end coordinates were specified by the allowed boundary deviation. This implies that if, for example, the boundary deviation was set to be 2 mol% then each line contained 81 segments (9 possible coordinates for each side).

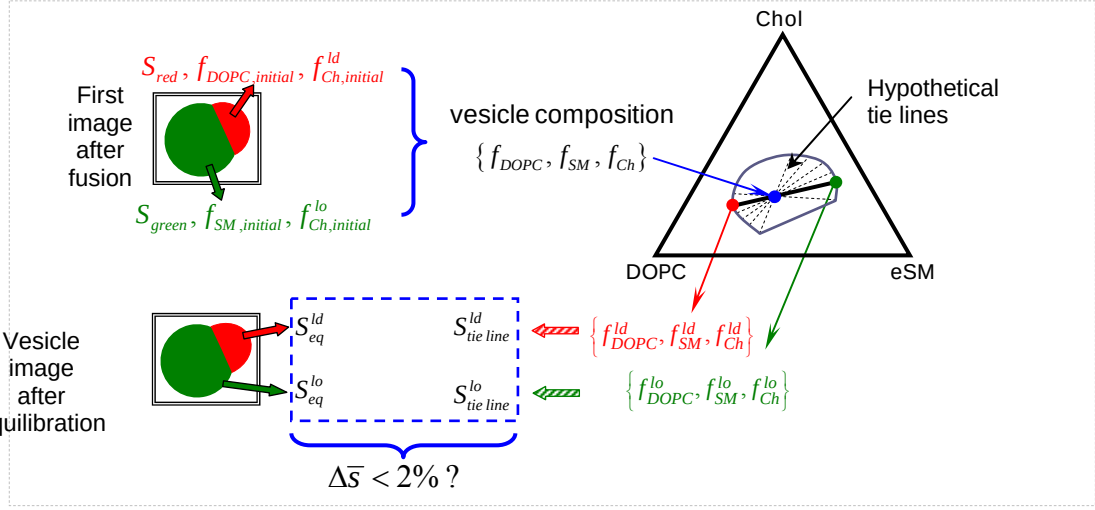

FIGURE S4 A schematic illustration of the procedure for searching for trial tie lines. From the first image collected right after fusion, we measure the areas of the domains. Knowing the domain composition and the area, we determine the total composition of the fused vesicle as marked by the blue circle in the phase diagram. Hypothetical tie lines are drawn through this compositional point. Their intersections with the boundary of the l_o-l_d coexistence region define the hypothetical compositions of the liquid phases in the equilibrated vesicle. From these compositions, the hypothetical areas of the equilibrated domains are calculated and compared to the areas of the domains measured in the image of the vesicle after equilibration following the selection criteria as explained in the text.

After allowing for boundary deviation, altogether 22857 trial tie-lines were found, yielding about 2×10^{22} possible sets of tie lines (intersecting and non-intersecting). Although the software was designed to search and select only non-intersecting lines, it would take too long to test and find this subset. To reduce the number of trial tie-lines, only one line segment for a given direction which gave minimal value of $\Delta\bar{s}$ was considered, if more than one segment on given line met the condition $\Delta\bar{s} < 2\%$. This condition reduced the number of trial tie lines down to 702. Manually this number was further reduced down to 250 lines by rejecting lines which clearly could not create any acceptable combination due to unavoidable intersection with neighboring tie lines; see Fig. S5A. The number of available combinations made from those 250 trial tie lines is about 5×10^{14} which is still too large to make the selection automatically. The trial tie lines which have minimal $\Delta\bar{s}$ do not form acceptable tie-line set since some of them intersect; see Fig. S5B. Therefore several trial tie lines with the

minimal $\Delta\overline{s}$ were taken as true tie lines for these points (shown as bold lines on Fig. S5B). For the rest of the points, the decision was made based on the selection criteria defined as the minimal sum of $\Delta\overline{s}$ and non-intersection with already available tie lines. Figure 5 in the main text shows the final 13 tie lines in the coexisting l_o-l_d region that were determined in this way.

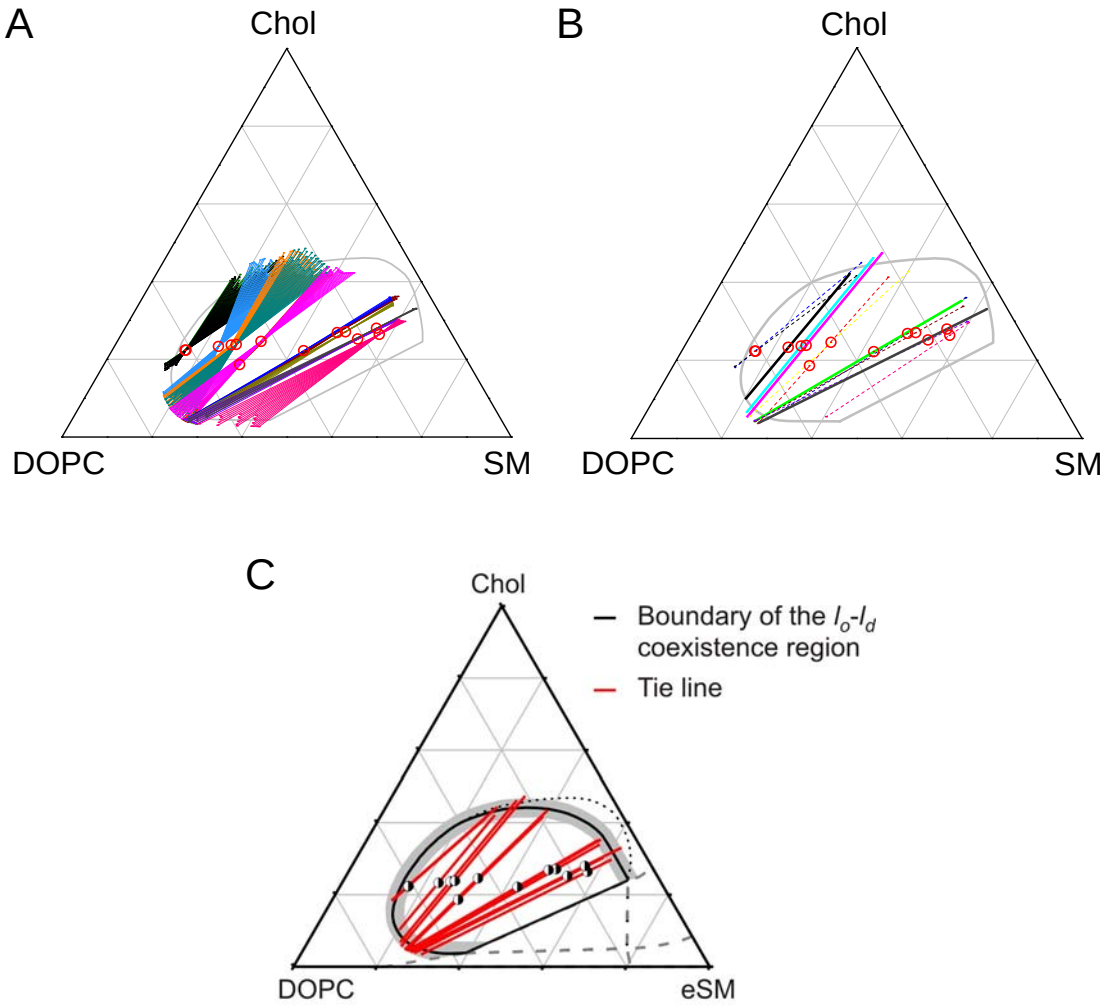

FIGURE S5 Tie lines in the l_o-l_d coexistence region. (A) All trial tie lines found for the composition points of the 13 fused vesicles (indicated with red open circles). The tie lines were selected under the condition that they do not cross the end tie line and that $\Delta\overline{s} < 2\%$, see text for details. The allowed deviation from the established coexistence curve was set to 2 mol% and 4.5 mol% from the binodals facing the single-phase l_d and l_o regions, respectively. (B) Trial tie-lines, one for each composition point, which have minimal $\Delta\overline{s}$, see text for details. (C) Final tie lines as in Fig. 5 in the main text.

Table S2 Coordinates of the found tie lines in the l_o-l_d coexistence region. The first column shows the composition of the vesicle used to determine the corresponding tie line. The last two columns show the angle between the tie line and the DOPC-eSM axis of the phase diagram and apparent free energies of lipid molecule transfer from the l_d to l_o phase.

Vesicle composition (DOPC/eSM/Chol)	Composition of the l_d phase			Composition of the l_o phase			Inclination angle of the tie line, °	Free energy of transfer, k_BT		
	DOPC	SM	Chol	DOPC	SM	Chol		ΔG^{DOPC}	ΔG^{SM}	ΔG^{Chol}
16:58:26	67.7	28.9	3.4	8.7	61.6	29.7	26.5	1.7	-1.1	-2.5
22:53:25	69.1	27.1	3.8	10.3	59.4	30.3	26.7	1.4	-1.3	-2.6
16:56:28	69.6	26.3	4.1	4.6	62.3	33.1	26.5	2.4	-1.1	-2.3
23:50:27	69.9	25.9	4.2	9.4	56.7	33.9	29.5	1.8	-1	-2.3
25:48:27	64.5	28.4	7.1	8.5	56.2	35.3	30.2	1.7	-1	-1.9
35:43:22	70.4	25.1	4.5	9.2	55.6	35.2	30.2	1.7	-1.1	-2.4
51:30:19	70.7	24.8	4.5	19.1	39.2	41.7	44.4	0.9	-0.8	-2.6
43:32:25	71.0	24.3	4.7	17.1	39.4	43.5	44.4	1	-0.9	-2.6
49:27:24	71.4	23.0	5.6	20.6	31.9	47.5	50.6	0.5	-1.1	-2.9
50:26:24	71.0	22.3	6.7	23.2	30.6	46.2	50.7	0.4	-1	-2.6
54:23:23	69.5	20.3	10.2	30.5	27.4	42.1	50.2	0.1	-1	-2.1
62:16:22	67.3	14.4	18.3	28.8	26.8	44.4	41.5	0.2	-1.2	-1.5
62:16:22	66.9	14.6	18.5	33.2	25.5	41.3	41.5	0	-1.3	-1.5

7. Creating multidomain vesicles

Consecutive electrofusion events allow us to create multidomain vesicles as shown in Fig. S6.

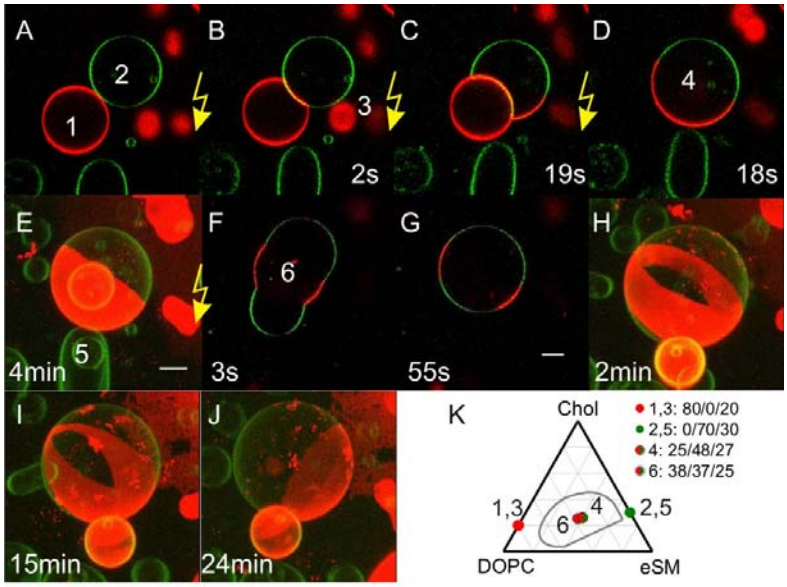

FIGURE S6 Formation of a three-domain vesicle by consecutive electrofusion of four vesicles (indicated with 1, 2, 3 and 5 in the images) with different compositions at 23°C. (A-D, F, G) Images acquired with confocal microscopy scans nearly at the equatorial plane of the fusing vesicles. (E, H-J) Three-dimensional projections. The sequence of pulses applied to the vesicles indicated with lightning symbol had the following amplitudes: 500kV/m, 300kV/m, 300kV/m, and 500kV/m. All pulses were 300 μs long. The time stamps indicate the time after each pulse. The scale bars correspond to 10 μm. (K) Phase diagram with the compositions of the six vesicles labeled from 1 to 6 in the confocal images.

References

1. Hell, S., and E. H. K. Stelzer. 1995. Lens aberrations in confocal fluorescence microscopy. In Handbook of biological confocal microscopy. J. B. Pawley, editor. Plenum Press, New York. 347-354.
2. Maulik, P. R., P. K. Sripada, and G. G. Shipley. 1991. Structure and Thermotropic Properties of Hydrated N-Stearoyl Sphingomyelin Bilayer-Membranes. Biochim. Biophys. Acta 1062:211-219.
3. Khelashvili, G. A., and H. L. Scott. 2004. Combined Monte Carlo and molecular dynamics simulation of hydrated 18:0 sphingomyelin-cholesterol lipid bilayers. J. Chem. Phys. 120:9841-9847.

4. Hofsäss, C., E. Lindahl, and O. Edholm. 2003. Molecular dynamics simulations of phospholipid bilayers with cholesterol. Biophys. J. 84:2192-2206.
5. Mathai, J. C., S. Tristram-Nagle, J. F. Nagle, and M. L. Zeidel. 2008. Structural determinants of water permeability through the lipid membrane. J. Gen. Physiol. 131:69-76.
6. Pan, J., S. Tristram-Nagle, N. Kucerka, and J. F. Nagle. 2008. Temperature dependence of structure, bending rigidity, and bilayer interactions of dioleoylphosphatidylcholine bilayers. Biophys. J. 94:117-124.
7. Smaby, J. M., M. M. Momsen, H. L. Brockman, and R. E. Brown. 1997. Phosphatidylcholine acyl unsaturation modulates the decrease in interfacial elasticity induced by cholesterol. Biophys. J. 73:1492-1505.